Supplementary Information for

Optical analogue of black and white gravitational holes

Eric Plum¹, Anton N. Vetlugin², Baurzhan Salimzhanov¹, Nikolay I. Zheludev^{1,2} and Nina Vaidya³

S1. Analytical description of optical black and white holes

We describe the optical properties of a device composed of a thin absorber layer placed in between two identical 90° prisms with an anti-reflection coating on the input face and surrounded by a medium with a refractive index of 1 (vacuum or air), as in Fig. S1. The special case of an absorber layer bisecting a pair of orthogonal mirrors corresponds to air-filled prisms with refractive index n=1 (Fig. S1 inset).

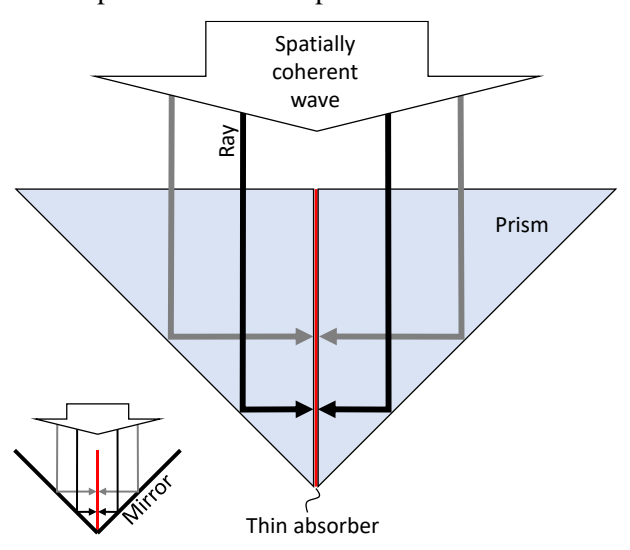


Figure S1. Optical black and white hole. A lossy thin film (red) bisects a pair of reflecting interfaces to form a compact 'interferometer' with matched optical paths. Spatially coherent waves of any wavelength will interfere in the same way (constructively or destructively) on the absorber, resulting in broadband coherent absorption or transmission. Waves transmitted through the absorber will be reflected by the device. Such absorber devices for light may be realized based on prisms (main graph) or mirrors (inset).

S1.1 Principle and ideal case

As discussed in the main text, constructive interference of waves incident on opposite sides of a lossy thin film enhances absorption in the film by enhancing the wave-matter interaction. This situation may also be described in terms of destructive interference of transmitted and reflected waves. A wave of amplitude E^i incident on one side of a planar absorber with transmission and reflection coefficients t and t will give rise to transmitted t and reflected t and reflected t waves. If these coefficients have equal amplitude and opposite phase, t and reflected t waves illumination of both sides of the absorber will yield complete cancellation of the transmitted and reflected waves on either side of the absorber, t and t which is known as "coherent perfect absorption". If t and t in the perfect transmission of the incident waves, known as "coherent perfect transmission".

¹ Optoelectronics Research Centre and Centre for Photonic Metamaterials, University of Southampton, Highfield, Southampton SO17 1BJ, United Kingdom

² Centre for Disruptive Photonic Technologies, SPMS, TPI, Nanyang Technological University, Singapore 637371, Singapore

³ Faculty of Engineering and Physical Sciences, Boldrewood Innovation Campus, University of Southampton, Southampton SO16 7QF, United Kingdom

For intermediate phases, the absorptivity oscillates between these extremes. The absorptivity A for coherent, counterpropagating incident waves of the same amplitude by such an ideal absorber layer (with t = -r = 0.5) is given by their phase difference θ at the absorber.

$$A = \frac{1}{2} + \frac{1}{2}\cos\theta\tag{S1}$$

The influence of prism misalignment Δz , polarization (s, p) and angle of incidence α on absorption is largely determined by their phase contributions, $\theta = \theta_{\Delta z} + \theta_{s/p} + \theta_{\alpha,s/p}$, and will be examined below.

S1.2 Real absorber materials

For an accurate description of coherent absorption and coherent transmission by a real thin film absorber with complex refractive index n_a and thickness d in an environment of refractive index n, the transmission and reflection coefficients can be derived from the Fresnel equations. At normal incidence and taking multiple reflections into account

$$t = \frac{4 n n_a e^{in_a kd}}{(n+n_a)^2 - (n_a-n)^2 e^{i2n_a kd}}$$
 (S2)

$$r = \frac{(n^2 - n_a^2)(1 - e^{i2n_akd})}{(n + n_a)^2 - (n_a - n)^2 e^{i2n_akd}}$$
(S3)

We note that it can be shown from Eq. (S2) and (S3) that t - r approaches 1 as the absorber's thickness d approaches 0.

For illumination from one side, the film's optical properties in terms of intensity are given by transmissivity $\tilde{T} = |t^2|$, reflectivity $\tilde{R} = |r^2|$ and absorptivity $\tilde{A} = 1 - \tilde{R} - \tilde{T}$. For coherent in-phase illumination with equal amplitude from both sides (i.e., constructive interference of the incident waves on the absorber), the absorptivity is given by

$$A_0 = 1 - |(r+t)^2| \tag{S4}$$

while for coherent out-of-phase illumination with equal amplitude from both sides (i.e., destructive interference of the incident waves on the absorber), the absorptivity is given by

$$A_{\pi} = 1 - |(r - t)^2| \tag{S5}$$

The absorptivity oscillates with phase between these extremes,

$$A = \tilde{A} + \Delta A \cos \theta$$
 with $\Delta A = \frac{A_0 - A_{\pi}}{2} = -2 \operatorname{Re}(r t^*)$ (S6)

Here we used that the average of absorptivity for in-phase and out-of-phase illumination of both sides of the thin film absorber equals its absorptivity for one-sided illumination, i.e., $\tilde{A} = \frac{A_0 + A_{\pi}}{2}$.

For the ideal case (with t=-r=0.5), $\tilde{A}=\Delta A=0.5$, $A_0=1$, $A_\pi=0$ and Eq. (S6) reduces to Eq. (S1). Real materials can come very close to the ideal case, with $A_0\approx 1$ and $A_\pi\approx 0$ across multiple octaves of the electromagnetic spectrum (Fig. S2), and data for various materials is available from https://refractiveindex.info/.

In the optical black hole configuration, 20 nm of chromium³⁹ are predicted to absorb more than 93% across the mid ultraviolet to near infrared spectral range (\leq 188 to \geq 1937 nm, \geq 3.4 octaves), indeed more than 98% absorptivity is predicted in the near infrared (676-1680 nm, 1.3 octaves). 20 nm of vanadium nitride⁴⁰ should absorb more than 96% from the far ultraviolet to the near infrared (150-2500 nm, 4 octaves), while absorptivity of 40 nm of graphite⁴¹ should exceed 98% in the mid infrared (1730 to \geq 10330 nm, \geq 2.6 octaves) and 99 nm of pyrolytic carbon⁴² is expected to absorb more than 98% in the near and mid infrared (1800-1600) nm, 5 octaves) and even more than 99.98% in the mid-infrared (1800-1600) nm, 2 octaves).

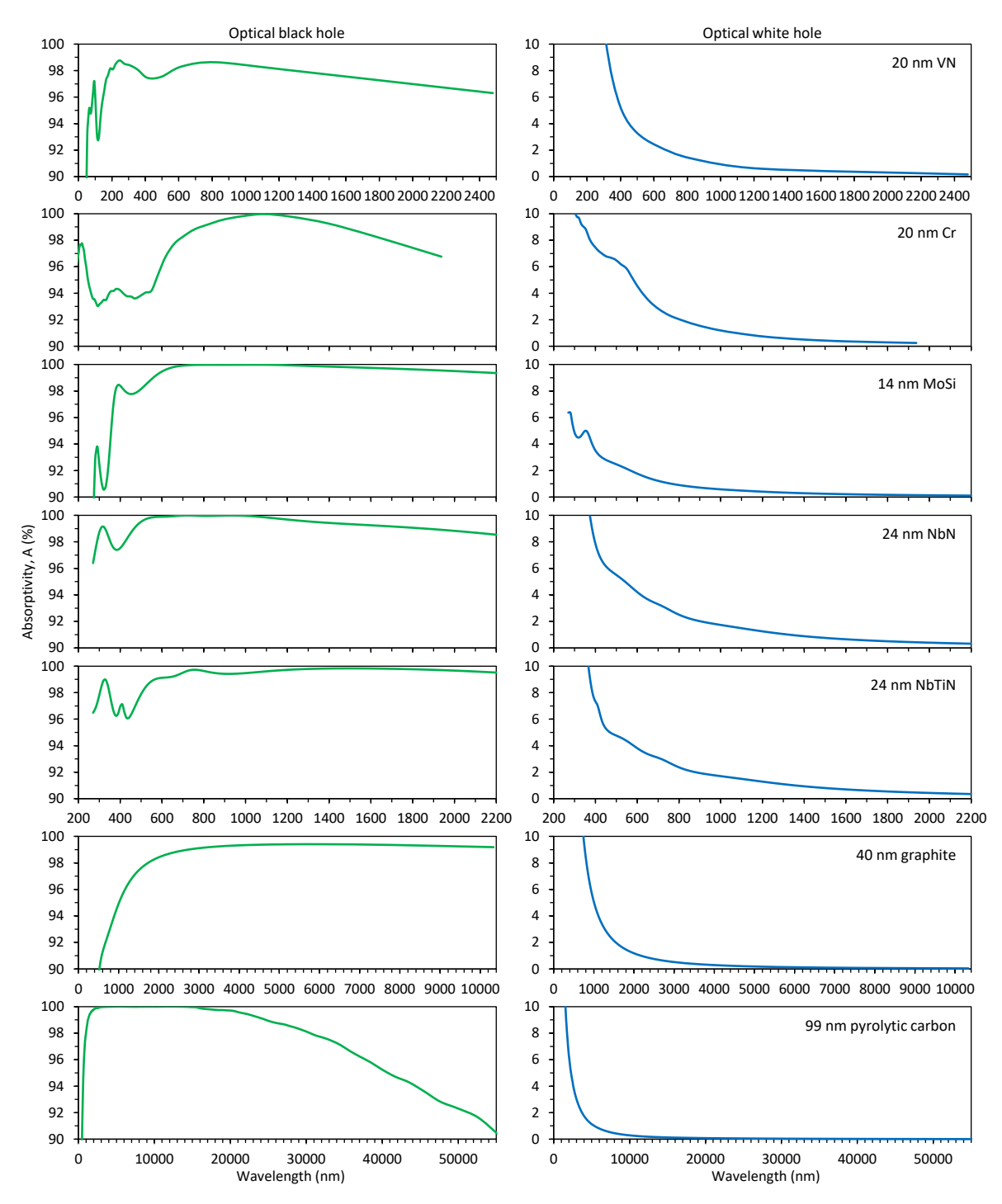


Figure S2. Theoretical absorptivity spectra of selected thin films in between identical prisms with refractive index 1.5 according to Eq. (S4) for the optical black hole case and Eq. (S5) for the optical white hole case using complex refractive index data for vanadium nitride⁴⁰, chromium³⁹, MoSi⁴³, NbN⁴³, NbTiN⁴³, graphite⁴¹ and pyrolytic carbon⁴².

For the white hole configuration, the calculations show that the absorptivity becomes negligible for wavelengths that are large compared to the optical thickness of the absorbing film. The absorptivity drops below 5% for wavelengths above 582 nm for 20-nm-thick chromium, above 410 nm for 20-nm-thick vanadium nitride, above 1005 nm for 40-nm-thick graphite and above 2280 nm for 99-nm-thick pyrolytic carbon. With increasing wavelength, the absorptivity asymptotically approaches zero, for example, dropping below 1% above 1080 nm for the chromium film and below 1% and 0.1% above 2175 and 6825 nm for the graphite film.

Further promising materials for the near ultraviolet to near infrared spectral range include NbTiN, NbN and MoSi,^{24,43} while broadband coherent absorption in the far infrared, terahertz and microwave spectral range has been predicted for appropriately doped silicon films.⁴⁴

These results indicate that extremely broadband optical black and white holes exhibiting near-complete absorption and reflection across several octaves of the electromagnetic spectrum can be realized with real materials, from the ultraviolet to the microwave spectral range.

S1.3 Prism alignment and polarization

For normal incidence of spatially coherent electromagnetic waves, the optical properties of the device are determined by interference on the absorber layer. If the prisms are perfectly aligned, then rays arriving at the same point on the absorber will have identical optical path lengths. A displacement Δz of one prism relative to the other will yield an optical path length change of Δz (Fig. S3a), i.e., a phase contribution $\theta_{\Delta z} = k \Delta z$ with $k = 2\pi/\lambda$. Therefore, with changing prism displacement, the interference on the absorber oscillates between constructive and destructive with a period of the wavelength λ , which will cause oscillations between large and small absorptivity.

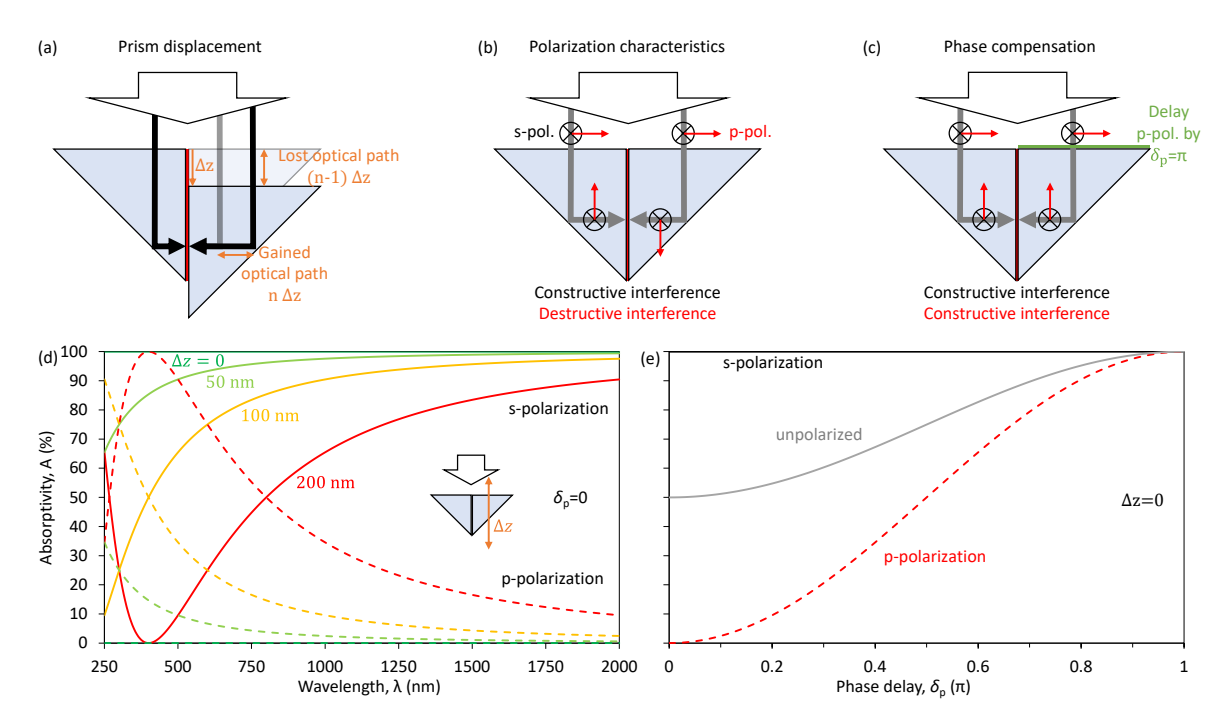


Figure S3. Polarization and alignment. (a) Optical path length change arising from a prism displacement Δz . (b, c) Interference of s-polarized (black) and p-polarized (red) waves without (b) and with (c) a birefringent layer (green) delaying p-polarization by a phase δ_p . (d) Absorptivity spectra for different prism displacements Δz , for s-polarization (solid) and p-polarization (dashed) without a birefringent layer, δ_p =0. (e) Absorptivity as a function of phase delay δ_p for different polarizations and aligned prisms, Δz =0. All results are shown for normal incidence, α =0, according to Eq. (S7) and (S8) assuming an ideal thin film absorber.

To derive the device absorptivity, we need to consider how different polarizations are reflected within an aligned device (Fig. S3b). For s-polarization (black), where the electric field is perpendicular to the plane of light propagation, the device geometry and electric fields are symmetric with respect to the plane of the absorber, resulting in constructive interference ($\theta_s = 0$) on the absorber and thus high absorptivity. However, for p-polarization (red), where the electric field is within the plane of light propagation, the direction of the incident electric field breaks said mirror-symmetry: The parallel electric field vectors of a pair in incident rays become anti-parallel after reflection within the device, resulting in destructive interference of p-polarized waves on the absorber ($\theta_p = \pi$) and thus low absorptivity.

Constructive interference of p-polarized waves would be achieved if an additional phase delay $\delta_p = \pi$ was applied to p-polarized waves incident on one of the prisms (such that $\theta_p = \pi + \delta_p$), e.g. by a

birefringent layer acting as a wave plate (Fig. S3c). Such a phase delay would invert the p-polarization electric field vector, resulting in mirror-symmetry (of device and electric fields) within the device.

Assuming lossless redirection of rays and prisms with anti-reflection coatings – the absorptivity for sand p-polarization is given by Eq. (S6) with the above phase contributions

$$A_{\rm S} = \tilde{A} + \Delta A \cos(\theta_{\Delta z} + \theta_{\rm S}) = \tilde{A} + \Delta A \cos\left(\frac{2\pi \Delta z}{\lambda}\right) \tag{S7}$$

$$A_{\rm p} = \tilde{A} + \Delta A \cos(\theta_{\Delta z} + \theta_{\rm p}) = \tilde{A} - \Delta A \cos(\frac{2\pi \Delta z}{\lambda} + \delta_{\rm p})$$
 (S8)

Thus, a perfectly aligned device without birefringent layer acts as a broadband polarizer, perfectly absorbing s-polarization (black hole), while reflecting p-polarization (white hole, Fig. 4, S3d). Introduction of a (superachromatic) birefringent layer would result in increasing absorptivity for p-polarization as the phase delay δ_p is increased towards π , resulting in perfect and polarization-independent absorption for δ_p = π (Fig. S3e). (Similarly, polarization-independent rejection of light would result if the phase delay of π was applied to s-polarization instead of p-polarization.)

S1.4 Angle of incidence

The device absorptivity depends on the angle of incidence α , as observed in Fig. 3. This dependence has two types of causes:

- 1. Oblique incidence introduces a path difference ΔP and an additional phase difference $\Delta \Phi$ (due to reflection at different angles) between rays directed to the same position on the absorber layer (Fig. S4a, black rays), affecting their interference and thus absorption.
- 2. Oblique incidence affects the counterpropagating absorber illumination for some pairs of incident rays, because
 - a. the absorber layer obstructs the path of some rays (Fig. S4a, red rays), such "obstruction" affects absorption of rays incident on a segment S of the input aperture,
 - b. some rays are directed to the absorber without a counterpropagating partner ray (Fig. S4b), such "orphaning" affects absorption of rays incident on a segment S/2 of the input aperture,
 - c. other rays miss the absorber layer altogether (Fig. S4b), such "deflection" affects the absorption of rays incident on a segment S/2 of the input aperture.

The segment *S* of the input aperture is

$$S = 2L \tan |\alpha'| \tag{S9}$$

with the prism's leg length L, refractive index n and the angle of refraction

$$\alpha' = \arcsin\left(\frac{\sin\alpha}{n}\right) \tag{S10}$$

In the interest of simplicity, we shall limit our considerations to **small angles of incidence**, for which the fraction of the input aperture that is affected by **obstruction**, **orphaning** or **deflection** is **negligible**, i.e., $S/L \ll 1$. For example, for a refractive index n = 1.5 and angles of incidence of $\alpha < 1^{\circ}$, we get S/L < 0.023, implying that less than 2.3% of the input aperture is affected by such effects. The **small incidence angle approximation**, that neglects obstruction, orphaning and deflection, is applied from here onwards. Small incidence angles also ensure that the expressions for the transmission and reflection coefficients at normal incidence, given by Eq. (S2) and (S3), remain good approximations.

In case of prism-based absorber devices, we further assume that they are either illuminated within the angle of total internal reflection or that an ideal reflective coating ensures lossless redirection of rays beyond that angle. We shall consider the cases of Gaussian beam and plane wave illumination of aligned absorber devices.

For a **Gaussian beam** (G) of effective size $\sigma_{\rm eff}$ that is large compared to any segment affected by obstruction ($S \ll \sigma_{\rm eff}$), but does not extend significantly beyond the input aperture ($2\sigma_{\rm eff} < L$)

$$A_{s/p}^{G} = 2 \int_{0}^{\infty} A_{coh,s/p}(x) G(x) dx$$
 (S11)

Here, $G(x) = \frac{1}{\sigma_{\rm eff}\sqrt{2\pi}} \exp\left(-\frac{x^2}{2\sigma_{\rm eff}^2}\right)$ is the projection of the incident Gaussian beam on the input aperture. The incident beam's size is σ , its $1/e^2$ diameter is D= 4σ and its projected size on the input aperture is

$$\sigma_{\rm eff} = \sigma/\cos|\alpha|.$$
 (S12)

The coherent absorption $A_{\text{coh,s/p}}$ is determined by the phase difference θ of rays directed to the same position on the absorbing layer, with a contribution $\theta_{\alpha,s/p} = \theta_{\Delta P} + \Delta \Phi_{s/p}$ from the angle of incidence. $\theta_{\Delta P} = k \Delta P$ with $k = 2\pi/\lambda$ arises from a path difference $\Delta P = 2x \sin \alpha$, where x is the distance of a ray from the centre of the segment S on the input aperture. (It can be shown that the path lengths inside the prisms are always matched.)

$$A_{\text{coh,s}} = \tilde{A} + \Delta A \cos(\theta_{\alpha,s} + \theta_s) = \tilde{A} + \Delta A \cos(k \Delta P + \Delta \Phi_s)$$
 (S13)

$$A_{\text{coh,p}} = \tilde{A} + \Delta A \cos(\theta_{\alpha,p} + \theta_{p}) = \tilde{A} - \Delta A \cos(k \Delta P + \Delta \Phi_{p} + \delta_{p})$$
 (S14)

 $\Delta\Phi_s$ and $\Delta\Phi_p$ are the phase differences resulting from reflection at different angles of incidence (45° \pm α'). In case of total internal reflection, a larger phase advance results from a larger angle of incidence onto the totally internally reflecting interface, causing ΔP and $\Delta\Phi$ to have the same sign. For total internal reflection⁴⁵

$$\Delta\Phi_{\rm S} = \Phi_{\rm S} \left(\frac{\pi}{4} + \alpha'\right) - \Phi_{\rm S} \left(\frac{\pi}{4} - \alpha'\right) \quad \text{with} \quad \Phi_{\rm S}(\beta) = 2 \arctan \frac{\sqrt{n^2 \sin^2(\beta) - 1}}{n \cos(\beta)} \quad (S15)$$

$$\Delta\Phi_{\rm p} = \Phi_{\rm p} \left(\frac{\pi}{4} + \alpha'\right) - \Phi_{\rm p} \left(\frac{\pi}{4} - \alpha'\right) \quad \text{with} \quad \Phi_{\rm p}(\beta) = 2 \arctan \frac{n\sqrt{n^2 \sin^2(\beta) - 1}}{\cos(\beta)} \quad (S16)$$

After integration over the constant terms, Eq. (S11) for Gaussian beam absorption simplifies to

$$A_{\rm S}^G = \tilde{A} + \frac{\Delta A \sqrt{2}}{\sigma_{\rm eff} \sqrt{\pi}} \int_0^\infty (\cos(2kx \sin\alpha + \Delta\Phi_{\rm S})) e^{-\frac{x^2}{2\sigma_{\rm eff}^2}} dx$$
 (S17)

$$A_{\rm p}^G = \tilde{A} - \frac{\Delta A \sqrt{2}}{\sigma_{\rm eff} \sqrt{\pi}} \int_0^\infty \left(\cos(2kx \sin \alpha + \Delta \Phi_{\rm p} + \delta_{\rm p}) \right) e^{-\frac{x^2}{2\sigma_{\rm eff}^2}} dx$$
 (S18)

where $\sigma_{\rm eff}$ is given by Eq. (S12).

Fig. S4b illustrates the angular dependence of absorptivity according to Eq. (S17) for an ideal version of the experimental device (with an ideal absorber layer) and incident Gaussian beams of different 1/e² diameters. It shows how the acceptance angle of the absorber device opens up as the diameter of the incident beam decreases.

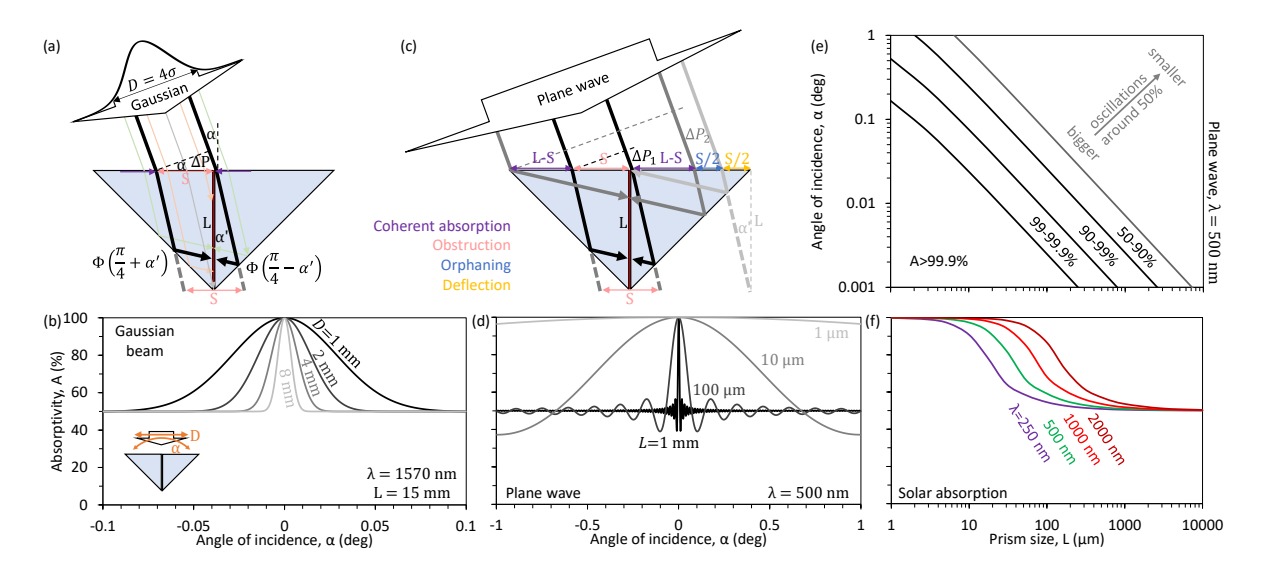


Figure S4. Angle of incidence. (a) Optical paths for a Gaussian light beam of $1/e^2$ diameter D incident at angle α on a pair of prisms of size L, resulting in optical path differences ΔP , assuming D < 2L. (b) Absorptivity as a function of angle of incidence for different Gaussian beam diameters according to Eq. (S17). (c) Optical paths for a plane wave incident on the prism pair at angle α , resulting in counterpropagating waves with optical path differences from ΔP_1 to ΔP_2 on the absorber. (d, e) Plane wave absorptivity as a function of angle of incidence for different prism sizes and green light according to Eq. (S19). (f) Direct sunlight absorptivity at representative wavelengths of the solar spectrum, calculated describing the sun as a circular source of plane waves with an angular diameter of 0.5° . Aligned glass prisms with an ideal absorber layer in all cases ($\Delta z = 0$, n = 1.5). All results are calculated assuming total internal reflection (including $\Delta \Phi_s$) for s-polarization, however, for $\delta_p = \pi$ results for any polarization closely resemble those shown.

For a **plane wave** (pw), still assuming that $S/L \ll 1$, the coherent absorption of Eq. (S13) and (S14) needs to be averaged across path differences from $\Delta P_1 = S \sin \alpha \approx 0$ to $\Delta P_2 = (2L - S) \sin \alpha \approx 2L \sin \alpha$, which yields

$$A_{\rm s}^{\rm pw} = \tilde{A} + \Delta A \frac{\cos(\hat{L} + \Delta \Phi_{\rm s})\sin(\hat{L})}{\hat{L}}$$
 (S19)

$$A_{\rm p}^{\rm pw} = \tilde{A} - \Delta A \frac{\cos(\hat{L} + \Delta \Phi_{\rm p} + \delta_{\rm p})\sin(\hat{L})}{\hat{L}} \tag{S20}$$

with $\hat{L} = kL \sin \alpha$, where integration was used for averaging and the difference identity for sines was used for simplification. For an ideal absorber $\tilde{A} = \Delta A = 0.5$.

It follows that the acceptance angle of the absorber device is strongly dependent on the prism size L. Macroscopic prisms yield high angular selectivity (e.g. for directional detectors), while microscopic prisms provide a large acceptance angle (e.g. for energy harvesting), see Fig. S4d,e. For example, the direct sunlight harvesting efficiency of an ideal device may be estimated by integration across the angular size of the sun (0.5°) , indicating that near-complete absorption of the solar spectrum would be achieved by (an array of) devices with prisms of size $L \leq 10 \, \mu m$ and $\delta_p = \pi$ (Fig. S4f).

However, redirection of light by total internal reflection is affected by scattering losses from prism edges, which allow an increasing proportion of the incident light to escape total internal reflection if the prism size is reduced. Such scattering losses become important for prism sizes below tens of wavelengths (Fig. S5a). If this is mitigated by a reflective coating (Fig. S5b), then the optical characteristics according to the ray optics description herein are preserved for prisms that are larger than the wavelength and the model only fails for sub-wavelength scale prisms, which would require a wave optics description.

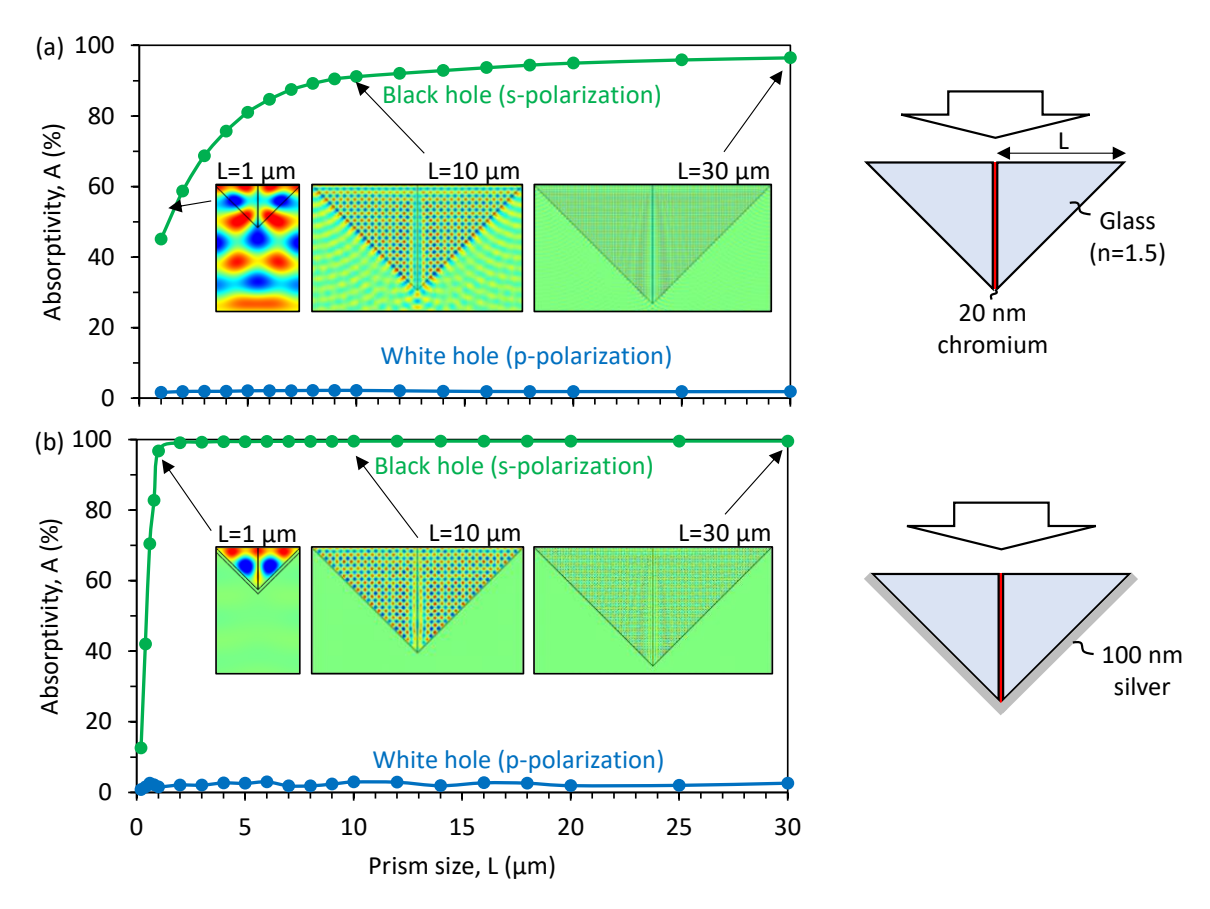


Figure S5. Coherent absorption and transmission as a function of prism size. Finite element method calculations (Comsol Multiphysics) for a chromium film of 20 nm thickness in between glass prisms with a refractive index of 1.5 and anti-reflection coated input faces, (a) without and (b) with an additional 100 nm silver layer on the reflective prism faces for normally incident plane waves and a wavelength of 1 μ m. The model uses periodic boundary conditions, i.e., it considers an array of prism pair devices. Field maps show the s-polarized electric field for selected prism sizes.

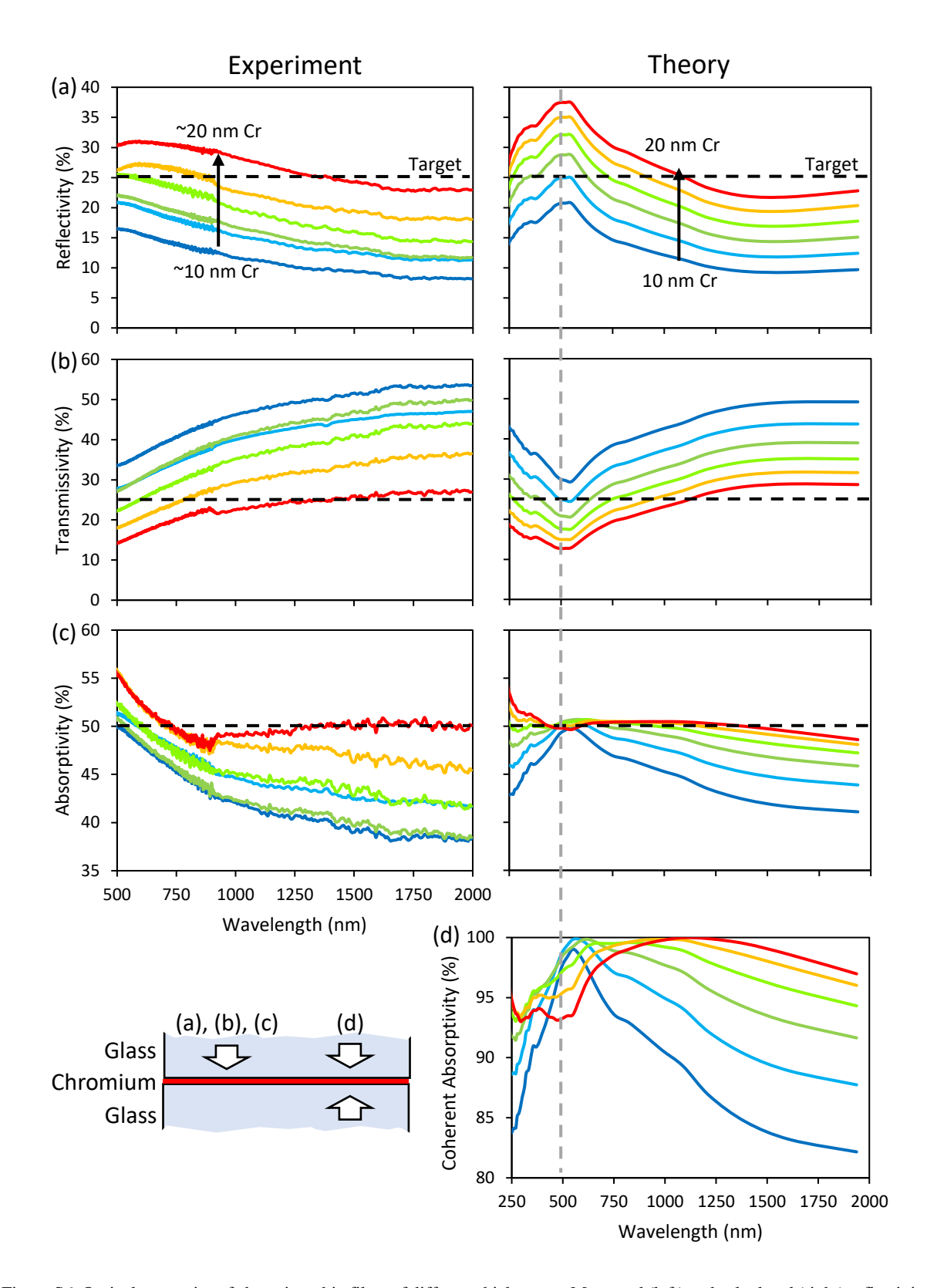


Figure S6. Optical properties of chromium thin films of different thicknesses. Measured (left) and calculated (right) reflectivity (a), transmissivity (b) and absorptivity (c) spectra of a glass/chromium/glass interface for illumination from one side, as well as calculated coherent absorptivity for simultaneous illumination from both sides (d). The theoretical results were calculated using the expressions in Section S1.2, the complex refractive index of chromium according to Johnson and Christy³⁹ and a refractive index of 1.46 for glass (to approximate the measurement conditions). For the experiments, chromium films with nominal thicknesses from 10 to 20 nm were thermally evaporated on glass substrates, covered with index matching liquid and a cover glass, and then characterized with a microspectrophotometer to identify the optimal thickness. Reflections at glass/air interfaces were taken into account to determine the optical properties of the chromium films.

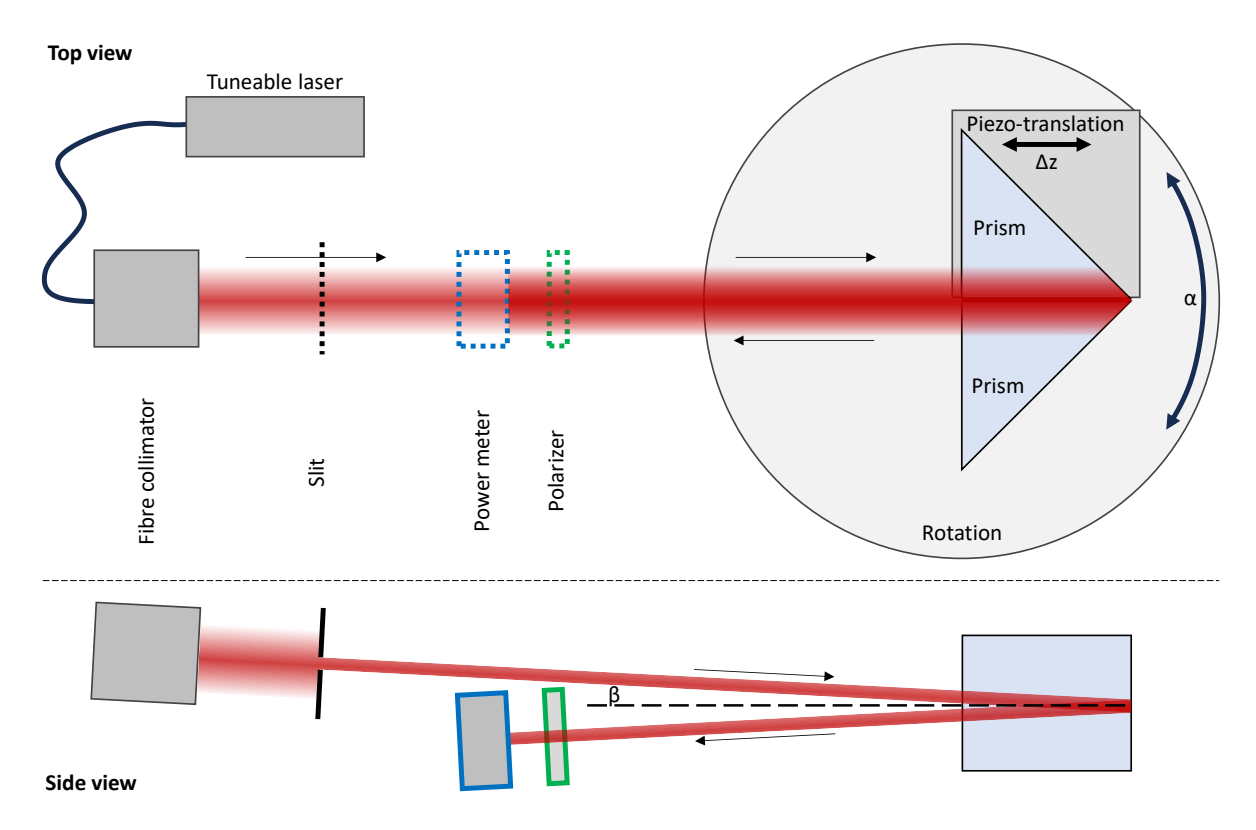


Figure S7. Top view and side view of the experimental setup.